Pharm Res (2013) 30:140–155
DOI 10.1007/s11095-012-0856-8

RESEARCH PAPER

Protein Antigen Adsorption to the DDA/TDB Liposomal Adjuvant: Effect on Protein Structure, Stability, and Liposome Physicochemical Characteristics

Mette Hamborg • Lene Jorgensen • Anders Riber Bojsen • Dennis Christensen • Camilla Foged

Received: 1 June 2012 / Accepted: 2 August 2012 / Published online: 6 September 2012

ABSTRACT

Purpose Understanding the nature of adjuvant-antigen interactions is important for the future design of efficient and safe subunit vaccines, but remains an analytical challenge. We studied the interactions between three model protein antigens and the clinically tested cationic liposomal adjuvant composed of dimethyldioctadecylammonium (DDA) and trehalose 6,6′-dibehenate (TDB).

Methods The effect of surface adsorption to DDA/TDB liposomes on colloidal stability and protein physical stability/secondary structure was investigated by dynamic light scattering, circular dichroism, Fourier transform infrared spectroscopy and differential scanning calorimetry.

Results Bovine serum albumin and ovalbumin showed strong liposome adsorption, whereas lysozyme did not adsorb. Upon adsorption, bovine serum albumin and ovalbumin reduced the phase transition temperature and narrowed the gel-to-liquid phase transition of the liposomes implying interactions with the lipid bilayer. The protein-to-lipid ratio influenced the liposome colloidal stability to a great extent, resulting in liposome aggregation at intermediate ratios. However, no structural alterations of the model proteins were detected.

Conclusions The antigen-to-lipid ratio is highly decisive for the aggregation behavior of DDA/TDB liposomes and should be taken into account, since it may have an impact on general vaccine stability and influence the choice of analytical approach for studying this system, also/especially at clinically relevant protein-to-lipid ratios.

KEY WORDS adjuvant · dimethyldioctadecylammonium · liposome · protein structure · vaccine delivery

ABBREVIATIONS

BSA	bovine serum albumin
CAF01	cationic adjuvant formulation 01
CD	circular dichroism
Cryo-TEM	cryo-transmission electron microscopy
DDA	dimethyldioctadecylammonium
DLS	dynamic light scattering
DSC	differential scanning calorimetry
FDA	Food and Drug Administration
FTIR	Fourier transform infrared
ISCOM	immune-stimulating complex
PDI	polydispersity index
TDB	trehalose 6,6′-dibehenate

INTRODUCTION

With the renewed societal and commercial interest in developing new prophylactic and therapeutic vaccines (1), there is a great need for addressing the pharmaceutical challenges associated with the vaccine development process. Modern subunit vaccines are composed of highly purified recombinant antigens, which by themselves are poorly immunogenic (2). Co-administration with efficient and safe

M. Hamborg (✉) • L. Jorgensen • A. R. Bojsen • C. Foged (✉)
Department of Pharmacy, Faculty of Health and Medical Sciences
University of Copenhagen
Universitetsparken 2
2100 Copenhagen Ø, Denmark
e-mail: mette.hamborg@sund.ku.dk
e-mail: camilla.foged@sund.ku.dk

D. Christensen
Department of Infectious Disease Immunology
Vaccine Adjuvant Research
Statens Serum Institut
Artillerivej 5
2300 Copenhagen S, Denmark

adjuvants is therefore often required to increase vaccine immunogenicity and efficacy. The introduction of recombinant protein antigens for sub-unit vaccines has resulted in much more well-defined and pharmaceutically acceptable vaccine formulations, compared to those previously used, and much more complex vaccines based on live attenuated pathogens (3). However, detailed characterization of the antigen-adjuvant mixtures still remains a poorly explored research area and an analytical challenge due to the particulate nature of most adjuvants and the relatively low protein antigen doses required for efficacy. A more thorough mechanistic understanding of the nature of antigen-adjuvant interactions is highly desirable, since this would allow for optimization of the efficacy and safety of vaccines, but also from a manufacturing point of view because such knowledge could help improve the overall formulation stability.

Over the past decade, a number of studies have described the effect on protein antigens' structure and physical stability upon their adsorption onto surfaces of the aluminum salt adjuvants, which are the most commonly used adjuvants and until recently were the only type of adjuvant registered by the Food and Drug Administration (FDA). The approach used to study these protein-adjuvant systems, which are characterized by a low protein content and their ability to cause particle-induced light scattering, has been to use a combination of low-resolution methods, such as Fourier transform infrared spectroscopy (FTIR), front face fluorescence, extrinsic fluorescence, UV spectroscopy and differential scanning calorimetry (DSC), to assess the antigen physical stability (4–9). However, very few studies have focused on characterizing the interactions between antigens and the lipid-based adjuvant systems (10–13), such as emulsions (oil-in-water and water-in-oil), immune-stimulating complexes (ISCOMs) and liposomes (14).

Self-assembling lipid-based particulate antigen delivery systems are complicated to analyse, due to their size and dynamic nature, but nevertheless constitute an integral part of many vaccine development programs. Compared to the solid alum salts, lipid-based adjuvants are flexible semi-solids, and therefore their interfaces available for antigen adsorption and the forces governing the adsorption process are very different from those of the alum salts. Antigens have been shown to adsorb to alum primarily through electrostatic interactions and ligand exchange (15), whereas protein adsorption to lipid-based delivery systems is believed to be governed by a combination of electrostatic and hydrophobic interactions, although hydrogen bond formation and van der Waals forces may also play important roles in both cases (2). Proteins are prone to partial unfolding when they are adsorbed to lipid-based particulate systems and expose their hydrophobic residues to accommodate to the new surroundings, represented by the oil–water interfaces (16). The primary method used to characterize antigen integrity in adjuvanted emulsions (e.g. Montanide®) has been SDS-PAGE, but this method cannot be used to assess the structural integrity of the protein antigen (10,13). In contrast, low-resolution methods, such as FTIR, fluorescence and circular dichroism (CD), which can be used to address structural changes, have seen limited use for the study of the structure of protein antigens in lipid-based adjuvant systems (12), probably due to the low protein content in vaccine formulation (usually below 100 μg/ml). However, these methods are frequently used to characterize lipid-based formulations designed for therapeutic proteins.

The lipid-based particulate adjuvant formulation addressed in the present study is a cationic liposomal adjuvant (CAF01, Statens Serum Institut, Denmark), which is based on the cationic surfactant dimethyldioctadecylammonium (DDA) and the immunopotentiator trehalose 6,6′-dibehenate (TDB), which is currently being tested in two clinical phase 1 studies with the tuberculosis fusion antigen Ag85B-ESAT6 (NCT ID: NCT00922363) and an HIV-1 peptide mix (NCT ID: NCT01141205; NCT01009762), respectively. Vaccination studies with CAF01 have been performed with surface adsorption of the antigens under study. It has been shown for the cationic DDA/TDB liposomes that antigens with an isoelectric point (pI) below 7 are readily adsorbed onto the liposome surface at physiological pH, whereas antigens with a pI above 7 have a low degree of adsorption (17). Therefore, attractive electrostatic interactions have been suggested to drive the adsorption process, which implies that adsorption might be influenced by the pI, charge distribution, and flexibility of the antigen, as well as the pH, ionic strength and composition of the buffer. In addition, a high degree of adsorption of the antigen has been shown to be important for the induction of Th1/Th17 responses, whereas adsorption is not a prerequisite for the stimulation of Th2 responses as well as antibody responses (17,18).

In this paper we characterize and discuss the interactions between antigens and DDA/TDB liposomes by varying the protein-to-lipid ratio. This is done in order to explore the system further and study its behaviour, also at protein doses above clinically relevant vaccine levels, which allows for the use of a wider range of biophysical methods. The aim is to improve the understanding of the nature of the interactions between DDA/TDB liposomes and protein antigens by applying the three model proteins bovine serum albumin (BSA), ovalbumin and lysozyme, which represent proteins of varying pI and size (Table I). A number of biophysical methods were applied to address further the analytical challenge of examining the antigen-adjuvant interactions. The colloidal stability was assessed by dynamic light scattering (DLS), the thermotropic phase behaviour of the liposomes was evaluated by DSC, and the integrity of the secondary structure was discussed based on results from FTIR and CD.

Table I Selected Physicochemical Properties of the Model Proteins Used in the Present Study (42–45)

Model protein	Mw kDa	Dimensions nm	pI
BSA	66	14 × 4.0 × 4.0	4.6
Ovalbumin	44	7.0 × 4.5 × 5.0	4.5
Lysozyme	14	4.5 × 3.0 × 3.0	11

MATERIALS AND METHODS

Materials

DDA was obtained from Avanti Polar Lipids (Alabaster, AL, USA). TDB was synthesized by Clausen-Kaas A/S (Farum, Denmark). The model proteins were obtained from Sigma-Aldrich (St. Louis, MO, USA); BSA (A7906, >98%), ovalbumin (A7641, 97%) and lysozyme (L6876, >90%). MeOH and $CHCl_3$ (extra pure) were purchased from VWR (Leuven, Belgium) and Merck (Darmstadt, Germany), respectively. Purified water of Milli-Q quality was used to prepare all buffers. Protein stock solutions were prepared in 10 mM Tris buffer (pH 7.4) and their concentrations were determined by UV spectroscopy at 280 nm with a NanoDrop spectrophotometer (Thermo scientific, Wilmington, DE, USA) using published extinction coefficients. The CAF01 adjuvant has an optimal stability in Tris buffer at pH 7.4, and although Tris buffer has a high temperature coefficient, all samples were prepared in 10 mM Tris pH 7.4 buffer to avoid altering the formulation.

Preparation of Liposomes by the Thin Film Method

The DDA/TDB liposomes were prepared by the thin-film method essentially as described previously (19), but with a few modifications. Briefly, weighed amounts of DDA and TDB were dissolved in $CHCl_3$-MeOH (9:1, v/v) in a round-bottomed flask, and the organic solvent was evaporated under vacuum resulting in the formation of a thin lipid film. The film was stripped twice with EtOH and dried overnight to remove trace amounts of the organic solvents. The lipid film was rehydrated with Tris buffer (10 mM, pH 7.4) and sonicated for 5 min using a Sonifier® cell disruptor (Branson, Danbury, CT, USA), followed by heating at 60°C for 60 min with 2 min of vigorous vortex mixing every tenth min. The final concentrations of DDA and TDB were 2.5 mg/ml (3.96 mM) and 0.5 mg/ml (0.51 mM), respectively, corresponding to a DDA: TDB molar ratio of 89:11. For the far UV CD measurements, the liposomes were prepared by the same procedure with one additional step; after 20 min of rehydration, the liposomes were tip-sonicated for 20 s with a 150 W Branson tip-sonicator (85% of the duty cycle) to reduce the size of the liposomes and thereby minimize the light scattering from the vesicles. The liposomes were stored at 4°C until further use.

Size, Polydispersity Index and Zeta Potential

The average liposome size distribution and polydispersity index (PDI) were analyzed by DLS using the photon correlation spectroscopy technique. The surface charge of the particles was estimated by analysis of the zeta potential (laser-Doppler electrophoresis). Equal volumes of protein solutions and liposome dispersions were mixed and left to equilibrate for 10 min. The lipid concentration was kept at 1.5 mg/ml (2.24 mM), while the protein solution was diluted two-fold and used in the concentration range of 0.01–10 mg/ml. The samples were then diluted five times, and left for 5 min (total dilution 10 times) before the size was measured. For the zeta potential measurements, the samples from the size measurements were diluted in total 300 times to a lipid concentration of 0.01 mg/ml. The measurements were performed in triplicate at 25°C using a Zetasizer Nano ZS (Malvern Instruments, Worcestershire, UK) equipped with a 633 nm laser and 173° detection optics. For viscosity and refractive index, the values of pure water were used. Malvern DTS v.6.20 software was used for data acquisition and analysis. A Nanosphere™ Size Standard (220 ± 6 nm, Duke Scientific Corporation, Palo Alto, CA, USA) and a zeta potential transfer standard (−50 ± 5 mV, Malvern Instruments, Worcestershire, UK) were used to verify the performance of the instrument. The particle size distribution was reflected in the PDI, which ranges from 0 for a monodisperse to 1.0 for an entirely heterodisperse dispersion.

Cryo-TEM

Morphological analysis was carried out by cryo-transmission electron microscopy (cryo-TEM) using a Philips CM120 BioTWIN transmission electron microscope (Philips, Eindhoven, Holland). Samples for cryo-TEM were prepared under controlled temperature and humidity conditions within an environmental verification system. A small droplet (5 μl) of sample was deposited onto a Pelco Lacey carbon-filmed grid. The droplet was spread carefully, and excess liquid was removed with a filter paper, resulting in the formation of a thin (10–500 nm) sample film. Then, the samples were immediately plunged into liquid ethane at −180°C. The vitrified samples were subsequently transferred in liquid nitrogen to an Oxford CT3500 cryo holder connected to the electron microscope. The sample temperature was continuously kept below −180°C. All observations were made in the bright field mode at an acceleration voltage of 120 kV. Digital pictures were recorded with a Gatan Imaging Filter 100 CCD camera (Gatan, Pleasanton, CA, USA).

Adsorption Isotherms

Equal volumes of protein solutions and a 3 mg/ml liposome dispersion were mixed in 1.5 ml low adsorption Eppendorf tubes and left to equilibrate for approximately 10 min at room temperature. The samples were then centrifuged at 25,000 g for 15 min at 4°C in an Eppendorf Centrifuge 5417R (Eppendorf, Hamburg, Germany). The protein concentration in the supernatant was determined by UV absorption at 280 nm. The amount of liposome-adsorbed protein was calculated by subtracting the amount of protein remaining in solution from the amount of protein initially added to the liposome dispersion.

Differential Scanning Calorimetry

The thermal stability of the model proteins and the gel-to-liquid crystalline phase transition temperature (T_m) of the vesicles in suspension were determined by DSC. Equal volumes of liposome dispersion and protein solution in 10 mM Tris buffer pH 7.4 were mixed. All samples and buffer were degassed prior to the measurements. The thermograms were recorded with a Microcal VP-DSC calorimeter (Northhampton, MA, USA) at a scanning rate of 1°C/min in the temperature range of 20°C to 110°C for protein analysis. A buffer scan was performed between each sample scan to ensure sufficient cleaning of the sample chamber. For determination of the phase transition of the vesicles, the samples were prepared as described above with final protein concentrations in the range of 0.01–7.5 mg/ml. Data collection was performed using a Nano DSC (TA instruments, New Castle, DE, USA) at a scanning rate of 0.5°C/min in the temperature range of 20°C to 60°C. VPViewer 2000 and Origin® 7 scientific plotting software (Origin Lab Corporation, Northampton, MA, USA) were used for baseline correction and data analysis, which were performed on the first of three scans of each sample (n=3). The T_{max} is the temperature at which the excess heat capacity, C_p, is at its maximum. The change in enthalpy (ΔH) was determined by integrating the area under the baseline-corrected C_p curve obtained for each sample.

Circular Dichroism

Far-UV CD measurements were performed at 22°C in a 0.1 mm quartz cell using an Olis DSM 10 Spectrophotometer (Olis, Bogart, GA, USA). The samples contained proteins at concentrations in the range of 0.1 to 0.8 mg/ml, and the lipid concentration was kept constant at 0.15 mg/ml. The samples were prepared 30 min prior to the measurements. All spectra were recorded from 200 to 250 nm using a step size of 0.5 nm, a fixed bandwidth of 0.5 nm and a constant integration time of 3 s resulting in a scan speed of 5 nm/min. All spectra were an average of three scans and were background-corrected and transformed into mean residue ellipticity [θ]. The shown spectra have not been smoothed. For control purposes, heat denatured protein samples were prepared by heating BSA and ovalbumin for 30 min in a water bath at 95°C. Lysozyme was heated at 95°C for 120 min. The heat-denatured proteins were also used as denatured controls for the FTIR measurements (see below).

Fourier Transform Infrared Spectroscopy

Infrared spectra were recorded using a Bomen MB 104 IR spectrophotometer (ABB, Bomem, Quebec, Canada), as described previously (16). The samples (12 μl) were placed in a cell of CaF_2 crystal windows with a path length of 6 μm. For each spectrum, a 256-scan interferogram was collected in the single-beam mode with a 4 cm^{-1} resolution at room temperature. Background spectra (either the Tris buffer and/or the DDA/TDB liposomes in Tris buffer) were subtracted from the spectra of the protein:DDA/TDB formulations to obtain a flat baseline in the region of 1850 to 2200 cm^{-1}. The spectra of the Tris buffer/ liposome dispersions were subtracted in the region of 1800 to 2600 cm^{-1}, and the water vapor spectra in the region of 1500 to1700 cm^{-1}. The second derivative spectra were obtained with a 13-point Savitsky-Golay derivative function, and the baseline was corrected using a three- to four-point adjustment. In addition, all spectra were area-normalized in the amide I region from 1595 to 1705 cm^{-1} using the Bomem-Grams software (Galactic Industries, Salem, NH, USA). The spectra obtained for the different formulations were compared using the area overlap method, as described previously (20).

RESULTS

Preparation and Characterization of DDA/TDB Liposomes

The physicochemical characteristics of the DDA/TDB liposomes were studied by DLS and laser-Doppler electrophoresis. The DDA/TDB liposomes prepared by the thin film method were relatively large and polydisperse multilvesicular vesicles with an average particle diameter between 600 and 900 nm and a PDI of 0.3 to 0.4 (results not shown), as reported previously (19). The vesicles prepared for the CD measurements with the additional sonication step during the rehydration process had an average particle diameter of 140±9 nm (n=3) and a PDI of 0.25±0.01 (n=3, results not shown). Cryo-TEM micrographs confirmed that smaller-sized, unilamellar DDA/TDB liposomes were formed as a result of the preparation procedure with the additional

sonication step (results not shown). Independently of the preparation method, the DDA/TDB liposomes had a high positive zeta potential of approximately + 60–80 mV, as reported previously (results not shown).

Quantification of Antigen Adsorption

The amounts of model proteins adsorbed to the DDA/TDB liposomes were estimated from adsorption isotherms (Fig. 1). Adsorption isotherms were only obtainable for BSA (pI of approximately 4.6) and ovalbumin (pI of approximately 4.5), but not for lysozyme because the vesicles mixed with lysozyme could not be sedimented at the centrifugation force used. Cationic DDA-based liposomes have previously been shown not to sediment efficiently during centrifugation, even at high centrifugal forces (21). We hypothesized that the columbic attraction governing the adsorption process for BSA and ovalbumin is followed by aggregation, which will result in sedimentation of the larger aggregates upon centrifugation. Therefore, the adsorption isotherms shown in Fig. 1 are representative for the part of the adsorption process that causes subsequent aggregation of the liposomes into larger structures. The adsorption process for BSA and ovalbumin reached saturation above approximately 1.0 mg/ml (BSA) and 0.7 mg/ml (ovalbumin) in the presence of DDA/TDB liposomes at a lipid concentration of 1.5 mg/ml (Fig. 1a, b). These values correspond to a molar protein concentration of 0.016 mM for both BSA and ovalbumin.

The theoretical surface coverage was also estimated using the mean molecular area of DDA and the protein dimensions (Table I). Given a DDA mean molecular area in the solid phase of 0.401 nm^2 (22) and protein dimensions ranging from approximately 16 to 56 nm^2 (BSA) and 23 to 35 nm^2 (ovalbumin), the estimated stoichiometry is between 40 to 140 and 56 to 87 lipid molecules per protein molecule, respectively. The lower value corresponds to the protein being oriented vertically to the lipid membrane and the higher value corresponds to protein being oriented longitudinally parallel to the lipid membrane. The estimated theoretical surface coverage in the case of BSA is approximately 57–201%, and the surface coverage of ovalbumin is approximately 80–124%, based on the assumptions that i) all liposomes are unilamellar, ii) 50% of the lipids is available for binding on the outer leaflet of the liposomal membrane and iii) upon adsorption, the protein maintains its globular conformation and is oriented vertically or longitudinally parallel to the surface of the liposome. In the literature, the surface adsorption of BSA onto a solid flat hydrophilic surface has been reported to result in up to 95% coverage of the surface area of a densely packed monolayer (23). The above estimated values are in the same range and above. This suggests that a densely packed monolayer is possible if the proteins are vertically adsorbed to the surface of the liposomes, whereas the protein might compile into more than a monolayer on the surface of the liposomes

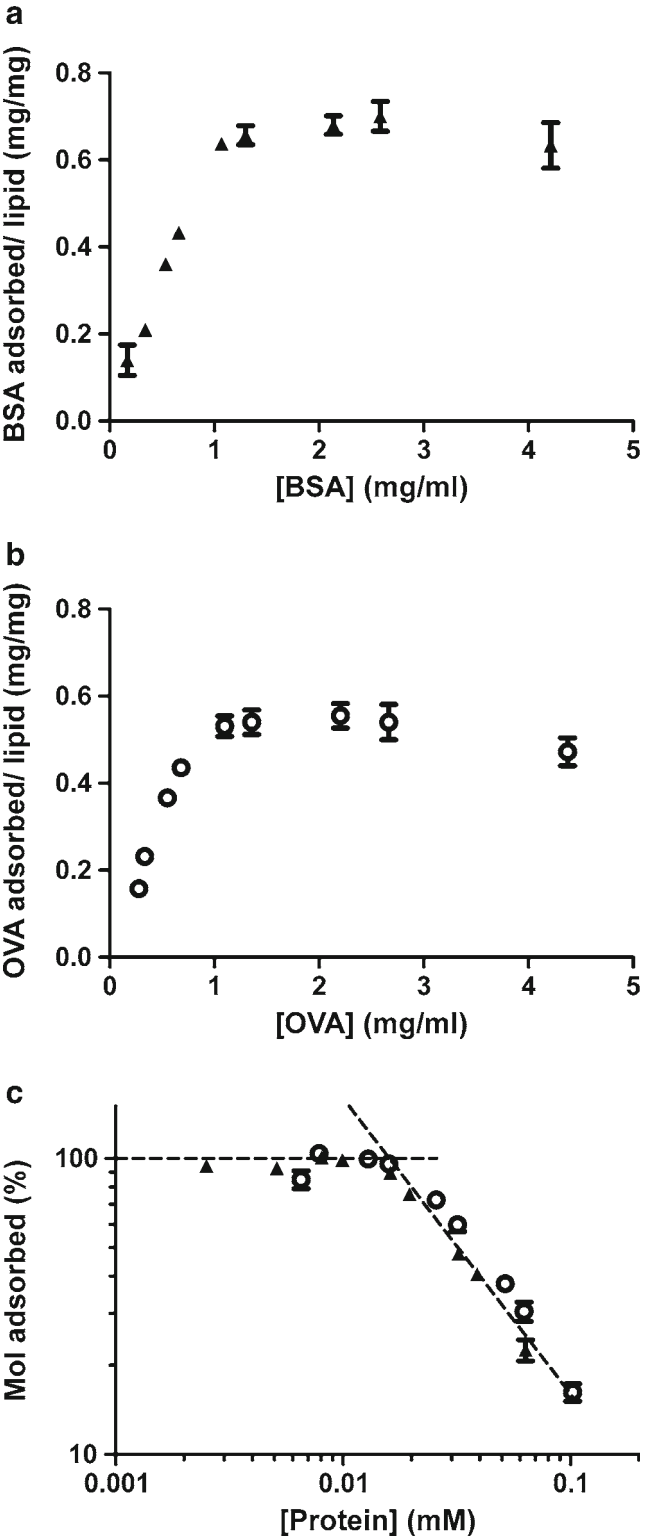

Fig. 1 Adsorption isotherms for the adsorption of (**a**) BSA and (**b**) ovalbumin to DDA/TDB liposomes. (**c**) The data from (**a**) and (**b**) presented as mol-percent of adsorbed protein. The results denote mean ± SD (n=3). For some data points, the standard deviations are too small to be seen.

if it is adsorbed in a different orientation. However, the liposome aggregation process occurring simultaneously with protein adsorption might reduce the surface area available for surface coverage. Nevertheless, the adsorption isotherms are characterized by a slope of approximately 1 (Fig. 1c), which indicates a constant surface area available for adsorption in the tested protein concentration range, despite the dynamic and flexible nature of the liposomes.

Addition of Protein Induces Aggregation of DDA/TDB Liposomes

To study further the overall effect of protein adsorption on the colloidal behavior of the liposome dispersion, DLS and laser-Doppler electrophoresis were applied. The results clearly confirmed that the cationic liposomes interacted strongly with the net negatively charged BSA and ovalbumin, whereas there was no measurable positive interaction with the net positively charged lysozyme (Fig. 2). This was foreseen, as the liposomes have a strong cationic net charge and the interaction is expected to be driven to a great extent by electrostatic attraction. However, the size measurements should only be taken as rough estimates, and they reflect the general stability of the liposome suspension after addition of protein. Upon aggregation, the particulate system becomes highly polydisperse. Comparing absolute values for the average particle diameter of such heterogenous systems would therefore be inappropriate. Nevertheless, the general trends in the average size of the particles in Fig. 2 reveal important and interesting features of the particulate system, which will be presented further below.

The size measurements showed that, in addition to the net charge of the protein, the protein-to-lipid ratio had a great impact on the colloidal stability of the liposomes. At low protein-to-lipid mass ratios, a modest increase in the particle diameter was observed upon addition of BSA and ovalbumin. However, at a protein-to-lipid mass ratio above 0.03 aggregation of the liposomes was induced (Figs. 2a, b). At the majority of the protein-to-lipid ratios tested, BSA and ovalbumin showed the same overall ability to induce liposome aggregation, except in the range from 3 mg protein per mg lipid and higher, where BSA seemed to stabilize the liposomes that had an average particle size of approximately 900 nm and a zeta potential of - 20 mV. This stabilization could be explained by adsorption of a protein layer to the surface of the liposomes, also referred to as a protein corona, as suggested for other types of nanoparticles interacting with serum proteins (24,25). In contrast, addition of ovalbumin at similar ratios and above did not prevent the liposomes from aggregating, though the zeta potentials were similar. A possible reason for this difference in the aggregation behavior could be that BSA forms a more dense protein layer around the liposomes (surface coverage of 201%) than the ovalbumin (surface coverage of approximately 112%) probably due to differences in their charge distribution and the flexibility of the proteins upon adsorption. The result is that the BSA-covered liposomes have a higher charge density than ovalbumin-covered liposomes, which might increase the colloidal stability.

To test the effect of initial particle size on the aggregation behavior of the liposomes, we examined the colloidal stability of smaller-sized, unilamellar liposomes with an average diameter of approximately 180 nm. The smaller liposomes had a greater capacity to adsorb protein, since more protein (up to 60 μg protein/mg lipid) could be added before liposome aggregation was induced (Figs. 2d, e). This increase can be explained by the larger available surface area for the smaller-sized liposomes, compared to the larger multivesicular vesicles, for which a larger fraction of the lipids is not accessible for protein binding.

The results presented above are in good accordance with previous observations for other types of charged liposomal systems showing that the protein (or peptide)-to-lipid ratio affects the colloidal stability as well as the secondary structure of the protein (26,27). Besides influencing the stability of the formulation, the aggregation behavior is also decisive for the choice of analytical method to study alterations in the secondary structure of adsorbed proteins, for instance, because the particle-induced light scattering phenomenon is a source of experimental problems for many spectroscopic methods.

BSA and Ovalbumin Interacts with the DDA/TDB Bilayer

The consequences of protein adsorption on the thermotropic phase behavior of DDA/TDB liposomes were studied further by DSC. Dispersions of DDA have previously been reported to have one sharp phase transition around 46.7°C (22). The thermogram for DDA/TDB liposomes, representing the gel-to-liquid phase transition, consists of two or more interconnected peaks between approximately 42°C and 47°C (Fig. 3A, scan a), suggesting that the two lipid components are inhomogeneously distributed, resulting in the existence of microdomains enriched in one of the two components of different heat transitions, as reported previously (19). Moreover, the thermotropic phase behavior of the liposomes was reversible, since the first and second scans were comparable (compare Fig. 3A and D, scan a). Upon addition of 1 mg/ml BSA, the phase transition was slightly narrowed and the T_m was decreased (Fig. 3A, scan c). At 4 and 7 mg/ml BSA, which are both above the surface saturation concentration, the peak was narrowed even further, and the T_m was markedly reduced to approximately 40°C (Fig. 3A, scan

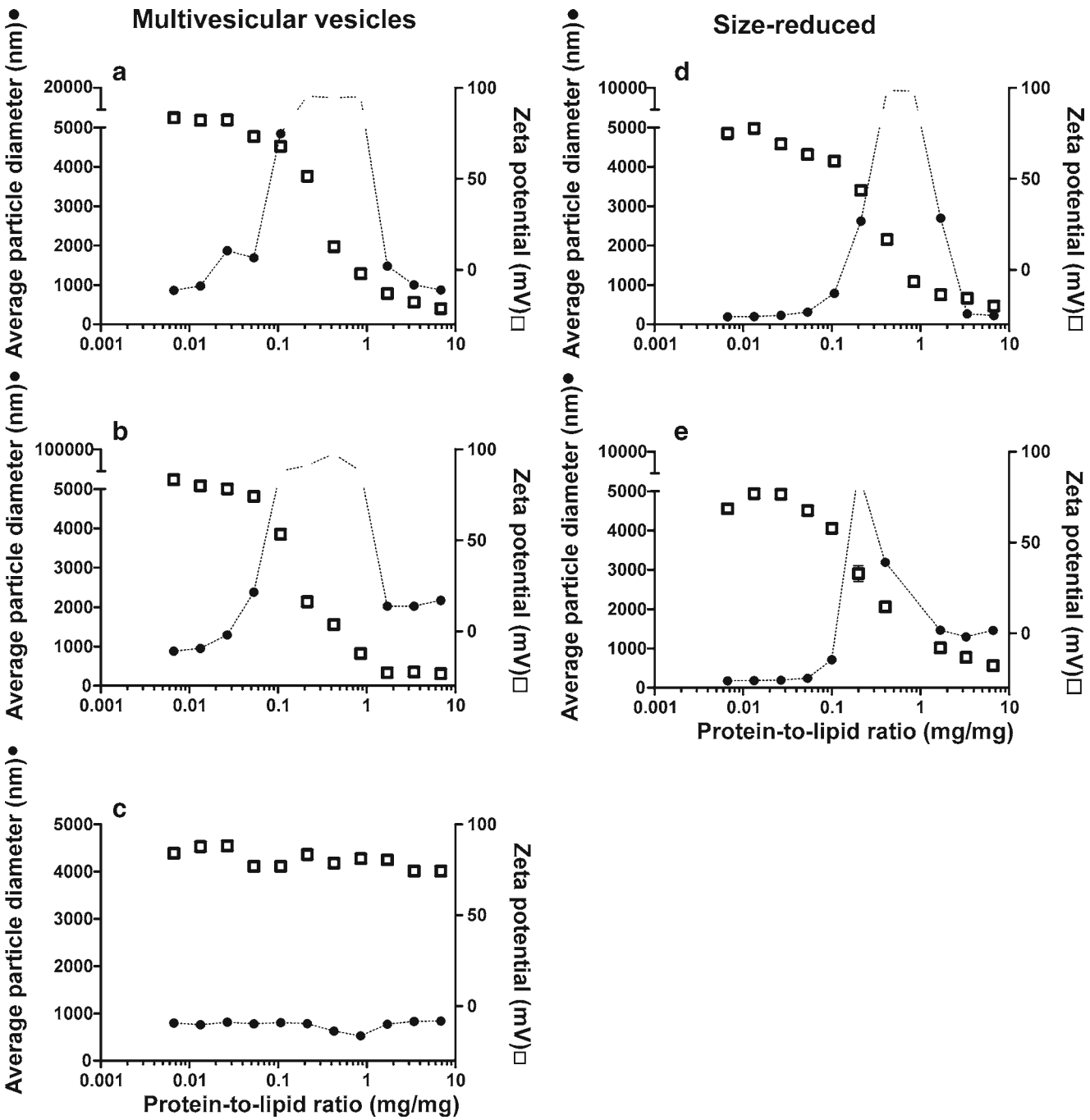

Fig. 2 Representative size and zeta potential of DDA/TDB liposomes (1250/250 μg/ml) upon addition of different concentrations of (**a**) BSA, (**b**) ovalbumin and (**c**) lysozyme, as well as size-reduced DDA/TDB liposomes (1250/250 μg/ml) upon addition of different concentrations of (**d**) BSA and (**c**) ovalbumin. In the ratio range of 0.1 to 1 (a and b), large aggregates outside the measurement range of the instrument were observed.

d and e). In addition, the reversibility of the liposome gel-to-liquid phase transition was lost (Fig. 3D, scans d and e). The decrease in the T_m and the loss of reversibility of the phase transition upon repeated heating and cooling suggested that the BSA was interacting not only with the lipid head group region, but also with the interfacial region of the bilayer and/or the apolar hydrocarbon chains in a way that disturbed the packing of the lipid molecules in the membrane and destabilized the lipid bilayer (28). The liposome bilayers might even have been disrupted, since the enthalpy of the gel-to-liquid phase transition was diminished (results not shown).

The addition of ovalbumin only affected the phase transition temperature to a small extent (Fig. 3B) and higher ovalbumin concentrations were required to narrow the transition peak and reduce the T_m, as compared to

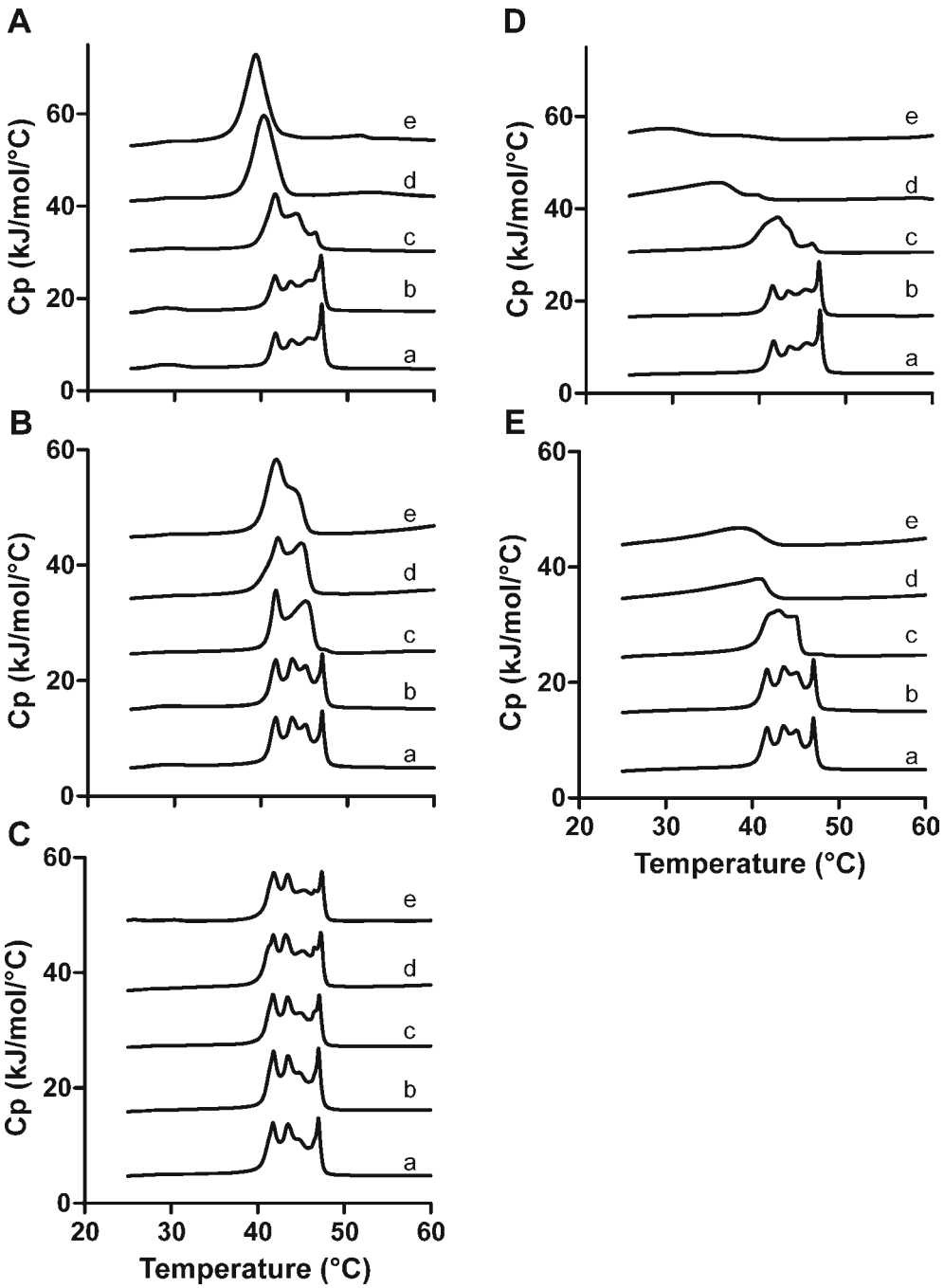

Fig. 3 Thermograms of DDA/TDB liposomal suspension ($n=2$) in the presence of different concentrations of (**A**) BSA, (**B**) ovalbumin and (**C**) lysozyme (first scan). Second scan in the presence of (**D**) BSA and (**E**) ovalbumin. The lipid concentration was 1.5 mg/ml and the protein concentrations were (**a**) 0 mg/ml, (**b**) 0.01 mg/ml, (**c**) 1 mg/ml, (**d**) 4 mg/ml and (**e**) 7.5 mg/ml.

BSA; addition of 4 mg/ml and 7.5 mg/ml ovalbumin resulted in a rearrangement of the lipids, characterized by a slight narrowing and shape change of the peak from four to two interconnected peaks (Fig. 3B). The phase transition was reversible at 0.01 mg/ml ovalbumin, but the reversibility was lost at 1 mg/ml ovalbumin and above (Fig 3E). This suggests that ovalbumin interacts not only with the head groups, but also with the apolar region of the lipid bilayer, and that the reversible nature of the transition is compromised due to this interaction, as observed for BSA (Fig. 3E). The observation that higher concentrations of ovalbumin are needed to decrease the T_m can be explained by the fact that ovalbumin is smaller and less hydrophobic, compared to BSA (29). The addition of lysozyme did not affect the gel-to-liquid phase transition (Fig. 3C). Thus, lysozyme did not show a measurable positive interaction with the DDA/TDB liposomes, which is in agreement with the observations from the adsorption isotherms and the colloidal stability studies (Fig 2c),

The Thermal Stability of the Protein Is Not Compromised by the DDA/TDB Liposomes

The consequences of liposome addition for the thermal stability of the proteins were also examined by DSC (Fig. 4 and Table II). The thermogram of the native BSA showed one peak at 71°C and a shoulder at higher temperatures, whereas the thermograms for ovalbumin and lysozyme were both dominated by only one peak at 77°C as reported in the literature (4). For both BSA and ovalbumin, there was no change in the T_{max} of the proteins, but the ΔH was markedly decreased at higher concentrations of lipid (Table II). The thermal stability of lysozyme was not influenced by the addition of liposomes, since neither changes in T_{max} and ΔH nor in the appearance of the diagrams could be observed (Table II and Fig. 4). Upon addition of DDA/TDB liposomes to BSA, the shoulder present at higher temperatures was diminished, whereas the T_{max} remained unchanged (approximately 72°C). The distinct exothermic peak at 90–95°C is often caused by protein aggregation (30,31). This was supported by the observed gel-formation of the samples that were withdrawn from the sample cell after the experiments.

The shape of the BSA thermogram changed markedly upon addition of liposomes at a lipid concentration of 0.75 mg/ml. Thus an unexpected exothermic peak appeared at 60°C, followed by a reduced endothermic peak at 72°C (Fig. 4A). The early exothermic peak might be explained by the instability of the colloidal system. The DSC studies were performed at a high protein-to-lipid mass ratio (>13), and according to Fig. 2a there is no aggregation at this mass ratio. Nevertheless, it is possible that the increased temperature disturbed the protein corona and caused liposome aggregation. This hypothesis was tested further by DLS, where the experimental conditions under which the samples were kept during the DSC study were simulated by heating to 90°C at the lowest protein-to-lipid mass ratio (approximately 13). This heating resulted in aggregation above 50°C (Fig. 5). In addition, aggregation of the samples with higher protein-to-lipid mass ratios did not occur until above 80°C, which also correlates well with the DSC results since no early aggregation exotherms were observed at these protein-to-lipid ratios.

The endothermic peak at 72°C reflects the unfolding of the bulk BSA not involved in the liposome aggregation process. The peak at approximately 40°C corresponds to the melting of the DDA/TDB liposomes, and the area of this peak was proportional to the lipid concentration. However, this T_m is slightly lower than that of DDA/TDB liposomes alone due to the interaction with the protein (Fig. 3). The thermograms of ovalbumin were not affected as much

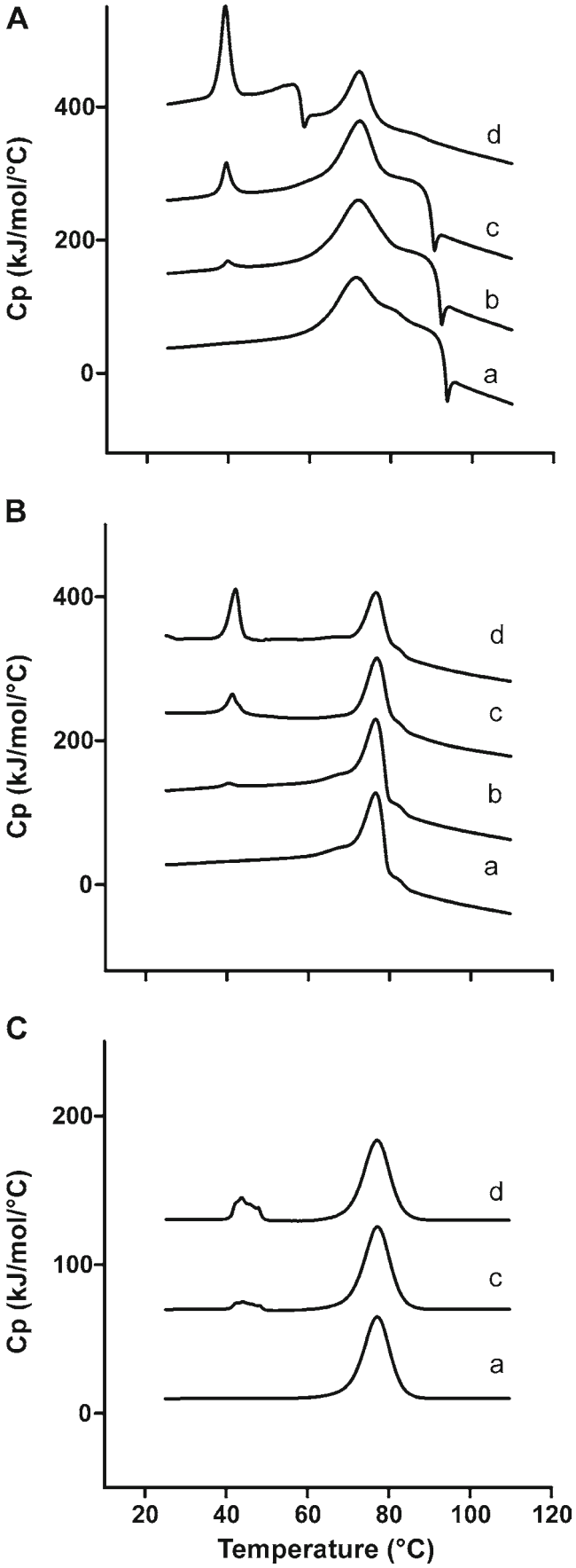

Fig. 4 Representative thermograms showing the thermal unfolding of (**A**) BSA, (**B**) ovalbumin and (**C**) lysozyme at 10 mg/ml in the presence of DDA/TDB liposomes at a final lipid concentration of a) 0 mg/ml b) 0.075 mg/ml, c) 0.3 mg/ml and d) 0.75 mg/ml.

Table II T_{max} Values and ΔH of BSA, Ovalbumin and Lysozyme in 10 mM Tris Buffer pH 7.4 in the Presence of DDA/TDB Liposomes (Data Represent mean ± SD, $n=3$)

DDA/TDB	BSA		Ovalbumin		Lysozyme	
Conc. mg/ml	ΔH kJ/mol	T_{max} °C	ΔH kJ/mol	T_{max} °C	ΔH kJ/mol	T_{max} °C
0	1059 ± 38	71.45 ± 0.06	859 ± 20	76.57 ± 0.26	473[a]	77.12[a]
0.075	1053 ± 12	71.92 ± 0.09	861 ± 15	76.73 ± 0.03	n.d.	n.d.
0.3	869 ± 66	72.30 ± 0.16	731 ± 53	76.91 ± 0.08	464[a]	77.20[a]
0.75	603 ± 28	72.19 ± 0.13	606 ± 37	76.85 ± 0.03	451[a]	77.05[a]

[a](n=1)
[n.d] not determined

as those for BSA upon addition of DDA/TDB liposomes. For ovalbumin alone, upon addition of liposomes at 75 μg/ml lipid, there was a shoulder present at a lower temperature, compared to the main peak at 77°C. This shoulder disappeared at higher DDA/TDB concentrations. The reduction of ΔH observed for both BSA and ovalbumin upon addition of DDA/TDB liposomes is related to changes in the unfolded state of the protein in the presence of DDA/TDB, compared to the unfolded state in the absence of lipid. From the studying of the phase transition of the DDA/TDB liposomes, we hypothesize that the proteins interacted with the hydrophobic hydrocarbon chains. This corresponds well with the reduction of ΔH of protein unfolding, because the unfolded protein interacts with the hydrophobic parts of the membrane, and this change the unfolded state of the protein, compared to the unfolded state in the absence of liposomes.

Charge-Mediated Adsorption to DDA/TDB Liposomes Does Not Induce Detectable Changes in the Protein Secondary Structure

In order to test whether the interaction between the liposomes and the protein influenced the secondary structure

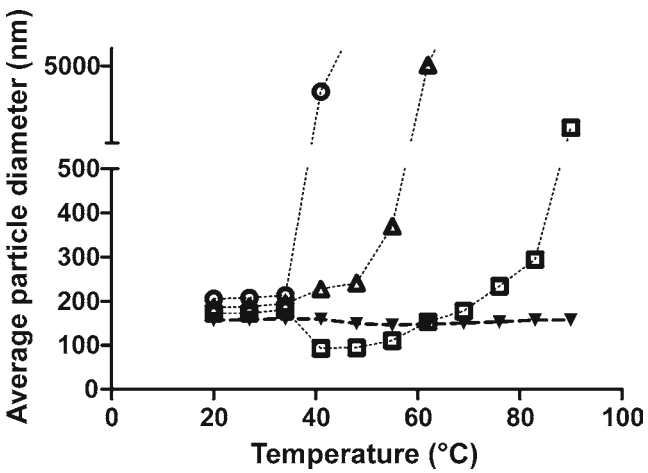

Fig. 5 Colloidal stability as a function of temperature of BSA (10 mg/ml) in the presence of DDA/TDB liposomes at a final lipid concentration of 0 mg/ml (▼) b) 0.3 mg/ml (□), 0.75 mg/ml (Δ) and 1.5 mg/ml (○).

of the protein, far-UV-CD and FTIR were applied. The spectrum of BSA showed a high content of α-helix structure, with strong negative CD signals at 208 and 222 nm (Fig. 6A), as previously reported in the literature (32,33). Upon addition of the size-reduced DDA/TDB liposomes (0.15 mg/ml lipid) to BSA (0.1 mg/ml), the negative signals at 208 and 222 nm were asymmetrically reduced, the signal at 208 nm being reduced more than the signal at 222 nm (Fig. 6A). At increased protein concentrations, the asymmetric shape of the spectra was maintained, though the signal strength was increased. This change induced by the addition of DDA/TDB liposomes might represent a loss of α-helix structure. However, it should be noted that data might be influenced by aggregation, since some spectra were recorded at protein-to-lipid mass ratios at which aggregation is known to take place according to Fig. 2d, e (the colloidally destabilized samples are marked with a star (*) in Fig. 6). This could complicate the spectral analysis and cause spectroscopic artifacts such as depolarization due to light-scattering and absorption-flattening effects (34–36).

The trends in the CD results for ovalbumin were highly similar to the results for BSA (Fig. 6B). Upon addition of DDA/TDB liposomes, the spectra were also markedly changed and the signal was decreased. For lysozyme, the addition of DDA/TDB liposomes apparently had no influence on the secondary structure of the protein (Fig. 6C). For positive control purposes, CD spectra were recorded of the unfolded proteins mixed with the DDA/TDB liposomes, in order to address the changes observed for the prepared samples. The data showed that the spectrum of unfolded BSA included a decreased signal, compared to the native BSA, with minimum at 208 nm. Upon addition of DDA/TDB liposomes, the CD signal was further reduced and the minimum at 208 nm was less pronounced. The CD spectrum of unfolded ovalbumin also showed a minimum at 208 nm, but the CD signal was not reduced. However, addition of DDA/TDB liposomes reduced the signal, and the minimum at 208 nm was flattened. The spectrum of unfolded lysozyme showed a reduced CD-signal with a minimum between 210–220 nm and, interestingly the spectrum was unchanged in the presence of DDA/TDB liposomes (0.15 mg/ml lipid). Based on these results, the asymmetric spectra of BSA and

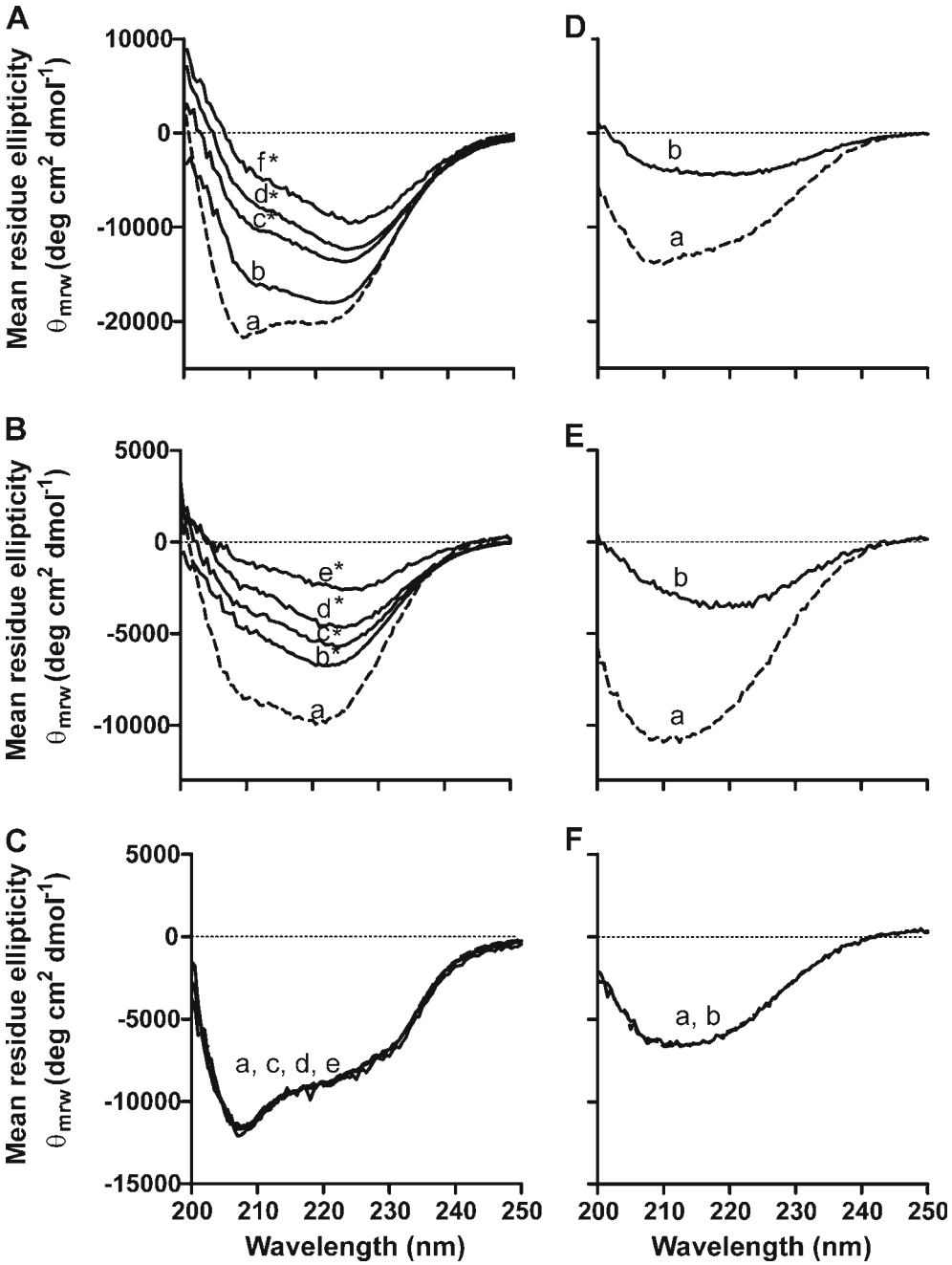

Fig. 6 Far-UV CD spectra recorded of (**A**) BSA, (**B**) ovalbumin and (**C**) lysozyme alone (**a**), and in the presence of liposomes (lipid concentration 0.15 mg/ml) at various protein concentrations [(**b**) 0.8 mg/ml, (**c**) 0.4 mg/ml, (**d**) 0.3 mg/ml, (**e**) 0.2 mg/ml and (**f**) 0.1 mg/ml]. Spectra recorded of heat aggregated (**D**) BSA, (**E**) ovalbumin and (**F**) lysozyme alone (**a**) and in the presence of liposomes (**b**). *Increased particle size of the liposomes in the sample due to liposome aggregation.

ovalbumin are likely to be a result of light-scattering artifacts, and it is therefore difficult to draw conclusions regarding changes in liposome-induced secondary structure based on CD measurements alone. In contrast, the spectrum of unfolded lysozyme was unchanged in the presence of DDA/TDB liposomes (Fig. 6). This suggests that CD is well-suited for non-aggregating systems, as shown for peptides in the presence of 100 nm liposomes (37).

Since the secondary structure could not be assessed properly using CD due to light-scattering artifacts, the secondary structure of the proteins upon adsorption was also studied by FTIR, which is commonly used to study structural changes of proteins in particulate formulations (5,7), due to the minor influence of particle-induced light scattering in the IR range of 4000 to 500 cm^{-1} (38). The spectrum for BSA is dominated by a large main peak at 1658 cm^{-1}, corresponding to α-helix (1648 to 1660 cm^{-1} (38)), since BSA is an α-helical protein. The band at 1658 cm^{-1} was similar both in the presence and absence of DDA/TDB liposomes, indicating similar amounts of α-helix (Fig. 7). In addition, there were no changes in the area overlap (0.96 ± 0.02 *versus* 0.87 ± 0.05), and hence DDA/TDB liposomes induced no or minor detectable changes in the secondary structure of BSA under the applied experimental conditions (Table III).

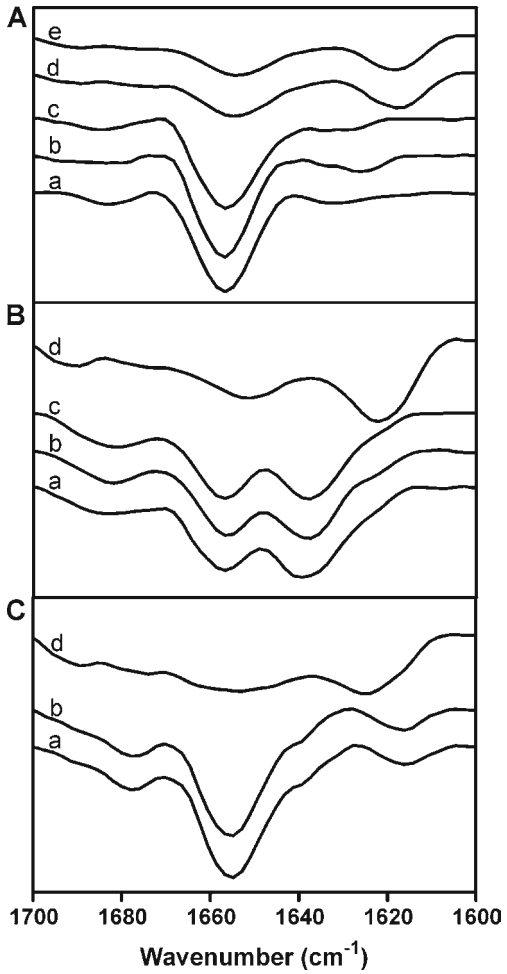

Fig. 7 FTIR spectra of (**A**) BSA, (**B**) ovalbumin and (**C**) lysozyme in 10 mM Tris buffer pH 7.4, alone (**a**), mixed with DDA/TDB liposomes (**b**), spun down in DDA/TDB pellet (**c**), and heat aggregated (**d**). As a control, heat aggregated BSA was mixed with DDA/TDB liposomes (**e**).

In order to improve the sample and exclusively determine the structure of the bound protein, the sample was sedimented and the protein structure was measured in the resulting pellet. Again, no structural changes were observed, and the area overlap was 0.96±0.02. The positive control consisting of heat-denatured BSA showed a reduction in the α-helix band at 1658 cm^{-1} and the presence of a band at 1620 cm^{-1}, corresponding to aggregated β-strands [1610–1628 cm^{-1} (38)] (Fig. 7). The spectrum for thermally unfolded BSA was highly similar upon mixing with DDA/TDB liposomes, which confirms that structural changes are in fact detectable by FTIR in the presence of liposomes.

Table III Area Overlap of Second Derivative FTIR Spectra of Native Proteins in 10 mM Tris Buffer pH 7.4 *Versus* in the Presence of DDA/TDB Liposomes, in the DDA/TDB Pellet and Heat Denatured (Data Represent mean ± SD, *n*=3)

	BSA	Ovalbumin	Lysozyme
In Tris buffer	0.96±0.02	0.98±0.02	0.95±0.01
Liposomes mixture	0.87±0.05	0.96±0.01	0.94±0.01
Liposome pellet	0.91±0.01	0.96±0.00	–
Heat aggregated	0.61±0.00	0.72±0.02	0.72±0.00

DDA/TDB liposomes also did not induce structural changes in ovalbumin (Fig. 7, Table III). The spectrum of native ovalbumin contained an α-helix band at 1658 cm^{-1} and a β-sheet band at 1639 cm^{-1} [1625–1640 (38)]. The bands were present both in the presence and absence of the liposomes. For denatured ovalbumin, the main band was found at 1620 cm^{-1}, corresponding to aggregated strands. The spectrum for lysozyme was dominated by an α-helix band at 1656 cm^{-1}, which upon heat denaturation resulted in a main band at 1625 cm^{-1}, corresponding to aggregated strands. As expected, lysozyme did not undergo any structural changes in the presence of DDA/TDB liposomes (Fig. 7 and Table III).

DISCUSSION

In this study, a thorough investigation was carried out of the interactions existing between three model antigens and the cationic liposomal adjuvant DDA/TDB in formulation. Vaccine formulations adjuvanted with DDA/TDB liposomes currently tested in the clinic (≤1.5 mg/ml lipid) contain antigen concentrations of 50 μg/ml and below (protein-to-lipid mass ratio of 0.03), whereas the formulations tested in preclinical studies are in the range of 1.5 mg/ml DDA/TDB lipid and contain antigen concentrations of 1–10 μg/ml (protein-to-lipid mass ratio of 0.0007–0.007). Thus, the protein concentrations in DDA/TDB-containing vaccine formulations are below the sensitivity limits of the commonly used low-resolution protein structure characterization methods. To approach this analytical challenge, we therefore studied the vaccine system at various protein-to-lipid mass ratios in order to obtain more information about the colloidal stability of the liposomes and the influence on the liposome membrane characteristics as well as the secondary structure of the antigen upon adsorption.

Based on the light-scattering results, which revealed a highly distinct aggregation behavior, depending on the protein-to-lipid-ratio, we identified several different overall physical states of the system, based on the colloidal stability of the liposomes and the antigen adsorption pattern (Fig. 8). Thorough knowledge about the apparent physical state of the system is important for the choice of analytical method and for the interpretation of the results. The first identified state is in the presence of a net positively charged protein like lysozyme (Fig. 8a). The system is stabilized by the electrostatic repulsions existing between both the liposomes and the proteins. At this state, no detectable amount of protein is adsorbed to the surface of the liposomes, and their size remains unchanged.

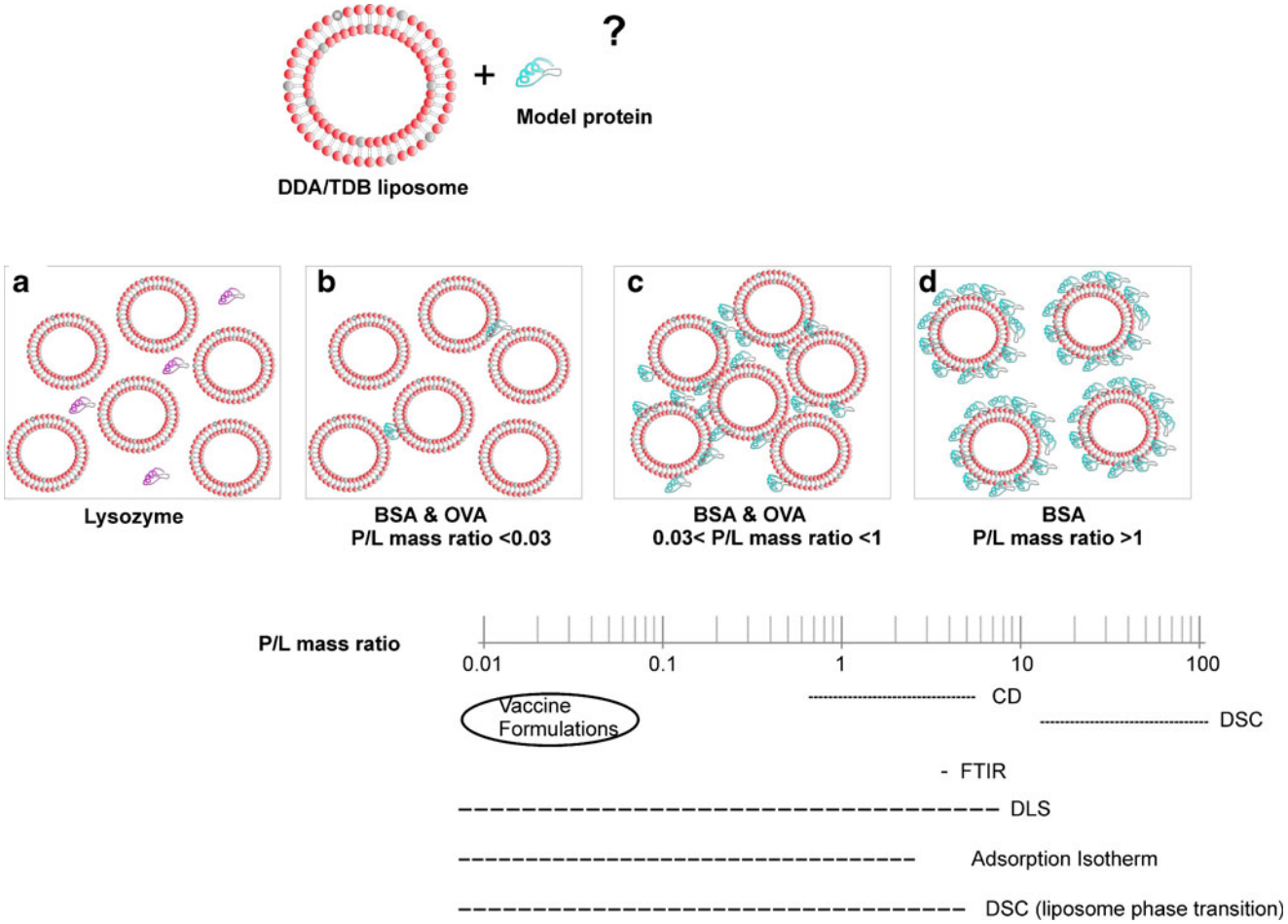

Fig. 8 A graphical overview of the influence of the protein-to-lipid-mass ratios (P/L mass ratios) and the analytical methods included in this study and the different physical states observed for the vaccine system. (**a**) Lysozyme and DDA/TDB liposomes: No measurable positive interaction. (**b**) At low concentrations of BSA/ovalbumin and DDA/TDB liposomes: No detectable aggregation (all the protein is adsorbed). (**c**) Intermediate concentrations of BSA/ovalbumin and DDA/TDB liposomes; Aggregation and partial adsorption of the protein. (**d**) High concentrations of BSA: The liposomes are stabilized by a protein corona and protein is present in bulk.

The second scenario is the interaction between DDA/TDB liposomes with net negatively charged proteins like BSA and ovalbumin at protein-to-lipid mass ratios below approximately 0.03, where the entire amount of added protein is adsorbed to the surface of the liposomes (Fig. 8b). However, the size of the liposomes is largely unchanged, as measured by DLS, although it cannot be excluded that the small amount of added net negatively charged protein could result in aggregation of a minor fraction of the liposomes. This physical state is probably the one that represents most closely a vaccine formulation used in the clinic.

The third apparent state is characterized by a higher concentration of net negatively charged protein, which induces liposome aggregation due to the presence of electrostatic attractive forces (Fig. 8c). The added protein may be adsorbed, but excess protein may also be present in bulk. The last scenario (Fig. 8d) is the complete coating of the head groups of the liposomes with the net negatively charged protein, resulting in the formation of a protein corona (24,25) that stabilizes the liposomes against aggregation, due to the electrostatic repulsions between the negatively charged proteins. This physical state was only evident for BSA, but not for ovalbumin. The protein-coated particles may coexist with unbound protein in bulk. As described previously, a possible reason why ovalbumin cannot fully stabilize this apparent physical state might be the difference in the surface coverage, since the adsorbed BSA layer has a higher surface coverage than the adsorbed ovalbumin layer.

Most of the analytical methods used in the current study to determine whether the presence of the liposomal adjuvant influenced the protein secondary structure were applied to samples at protein-to-lipid ratios resembling the last state (stabilized protein corona for BSA and partly stabilized protein corona for ovalbumin). These include FTIR, DSC (protein unfolding) and CD. Of the analytical methods investigated in this study, DLS, adsorption (yes/no) and

DSC (thermotropic behavior of the liposomes) were the only methods that could be applied at clinically relevant concentrations and protein-to-lipid ratios, which means that it is possible to measure the colloidal stability and the adsorption pattern (yes/no), but not the structural integrity of the antigen at vaccine relevant protein-to-lipid ratios. To assess the protein structure in lipid-based vaccine formulations, novel and better methods are greatly needed. Aggregation phenomena may compromise the results obtained with many of the spectroscopic methods commonly used to study protein structure, such as CD and fluorescence, due to light scattering-induced artifacts. Furthermore, it is an analytical challenge to have a sufficient protein concentration in the sample to overcome the lower limit of detection, which is approx. 0.1 mg/ml for CD and 5 mg/ml for the existing transmission FTIR equipment, but at the same time also to avoid determining the global protein structure, which is the average structure of a sample containing both bound and unbound protein in the bulk. This raises the dilemma of the choice of protein-to-lipid ratio. Ideally, for CD all the protein should be bound and no aggregates should be formed. On the other hand, FTIR is not as sensitive to light scattering, but samples containing both bound and unbound protein should be avoided so as not to average out structural changes.

This challenge has been overcome by drying antigen samples onto alum crystals, which allows for the study of interactions between alum and model protein samples at lower concentrations (0.5–1 mg/ml) using ATR-FTIR (5,7). Inspired by this study, we sedimented the liposome/adsorbed protein pellet in order to avoid measuring the structure of non-adsorbed protein in the bulk solution. However, this additional sample preparation step did not affect the monitored spectra, and no structural changes were observed. Altogether, no structural changes of the protein secondary structure could be measured in the presence of the liposomal adjuvant.

Above the phase transition temperature of the liposomes, however, the appearance of thermograms suggests that BSA and ovalbumin interact with the apolar hydrocarbon tails of the membrane, most likely through hydrophobic interactions as previously reported for proteins interacting with liposomes above the gel-to-liquid phase transition temperature (39,40). The interaction with the hydrophobic part of the membrane above the gel-to-liquid phase transition, and hence the likely change of the unfolded protein, could also be the reason for the observed decrease in the unfolding enthalpy of the proteins (BSA and ovalbumin) in the presence of liposomes (decrease of ΔH, Table II). Interestingly, lysozyme does not appear to interact with the lipid tail of the bilayer, suggesting that the protein needs to be adsorbed to the liposome surface through electrostatic interaction before the hydrophobic interactions can take place. We are currently addressing this further by systematically varying the surface charge of the liposomes. The observation that the interactions might include hydrophobic interactions above the phase transition temperature of the liposomes is important to consider during vaccine processing steps, such as spray-drying used for particle engineering of vaccines for pulmonary administration (41). During spray-drying, the formulation may briefly be heated to temperatures above the phase transition temperature of the liposomes, which based on our results may affect the bilayer structure of the liposomes and cause unfolding of the protein.

CONCLUSION

This study provides suggestions for how the interactions between lipid-based particulate adjuvant systems and model as well as clinically relevant antigens may be assessed. The analytical methods suitable for the study of clinically relevant cationic liposome-based formulations were DLS, adsorption (yes/no) and the thermotropic behavior of the vaccine. In order to measure the structural integrity of the adsorbed proteins, the protein-to-lipid ratio was increased, and this revealed that the colloidal stability of the formulations was highly dependent on the protein-to-lipid ratio, probably driven by attractive electrostatic interactions. Upon adsorption, BSA and ovalbumin interfered with the membrane fluidity suggesting interactions with the bilayer when the temperature was raised above the gel-to-liquid phase transition. However, at room temperature no structural changes of the proteins were observed, as expected upon interaction with the bilayer. For the liposome formulations containing lysozyme, no aggregation was found and no interaction with the bilayer was observed. This indicates that the electrostatic repulsions existing between the liposomes and lysozyme prevent the interaction and adsorption, also above the gel-to-liquid phase transition of the liposomes. The distinct aggregation behavior of the system is important, not only as it may affect the stability of the formulation but also for the analytical approach used to characterize the system.

ACKNOWLEDGMENTS AND DISCLOSURES

We are grateful to Fabrice Rose for excellent technical assistance and fruitful discussions during the preparation of this manuscript. The work was funded by the Faculty of Health and Medical Sciences, University of Copenhagen, Denmark and The Danish National Advanced Technology Foundation. We acknowledge the Danish Agency for Science, Technology and Innovation for the Zetasizer Nano ZS and The Danish National Advanced Technology Foundation and the Danish Ministry of Science, Technology

and Innovation for funding the nano-DSC. The Drug Research Academy, University of Copenhagen, is kindly acknowledged for funding the NanoDrop. Finally, we acknowledge Novo Nordisk A/S for co-funding the VP-DSC MicroCalorimeter. The funding sources had no involvement in the study design; in the collection, analysis and interpretation of data; in the writing of the paper; or in the decision to submit the paper for publication.

REFERENCES

1. Rappuoli R, Mandl CW, Black S, De Gregorio E. Vaccines for the twenty-first century society. Nat Rev Immunol. 2011;11:865–72.
2. Wilson-Welder JH, Torres MP, Kipper MJ, Mallapragada SK, Wannemuehler MJ, Narasimhan B. Vaccine adjuvants: current challenges and future approaches. J Pharm Sci. 2009;98(4):1278–316.
3. Volkin DB, Middaugh CR. Vaccines as physically and chemically well-defined pharmaceutical dosage forms. Expert Rev Vaccines. 2010;9(7):689–91.
4. Jones LS, Peek LJ, Power J, Markham A, Yazzie B, Middaugh CR. Effects of adsorption to aluminum salt adjuvants on the structure and stability of model protein antigens. J Biol Chem. 2005;280 (14):13406–14.
5. Dong A, Jones LS, Kerwin BA, Krishnan S, Carpenter JF. Secondary structures of proteins adsorbed onto aluminum hydroxide: infrared spectroscopic analysis of proteins from low solution concentrations. Anal Biochem. 2006;351(2):282–9.
6. Carra JH, Wannemacher RW, Tammariello RE, Lindsey CY, Dinterman RE, Schokman RD, *et al.* Improved formulation of a recombinant ricin A-chain vaccine increases its stability and effective antigenicity. Vaccine. 2007;25(21):4149–58.
7. Bai SF, Dong AC. Effects of immobilization onto aluminum hydroxide particles on the thermally induced conformational behavior of three model proteins. Int J Biol Macromol. 2009;45(1):80–5.
8. Ausar SF, Chan JD, Hoque W, James O, Jayasundara K, Harper K. Application of extrinsic fluorescence spectroscopy for the high throughput formulation screening of aluminum-adjuyanted vaccines. J Pharm Sci. 2011;100(2):431–40.
9. Soliakov A, Kelly IF, Lakey JH, Watkinson A. Anthrax sub-unit vaccine: the structural consequences of binding rPA83 to alhydrogel. Eur J Pharm Biopharm. 2012;80(1):25–32.
10. Miles AP, McClellan HA, Rausch KM, Zhu D, Whitmore MD, Singh S, *et al.* Montanide ISA 720 vaccines: quality control of emulsions, stability of formulated antigens, and comparative immunogenicity of vaccine formulations. Vaccine. 2005;23 (19):2530–9.
11. Jorgensen L, Wood GK, Rosenkrands I, Petersen C, Christensen D. Protein adsorption and displacement at lipid layers determined by total internal reflection fluorescence (TIRF). J Liposome Res. 2009;19(2):99–104.
12. Silva VD, Takata CS, Sant'Anna OA, Lopes AC, De Araujo PS, Da Costa MHB. Enhanced liposomal vaccine formulation and performance: Simple physicochemical and immunological approaches. J Liposome Res. 2006;16(3):215–27.
13. Xue XY, Ding F, Zhang QF, Pan XG, Qu L, Pan WQ. Stability and potency of the Plasmodium falciparum MSP1-19/AMA-1 (III) chimeric vaccine candidate with Montanide ISA720 adjuvant. Vaccine. 2010;28(18):3152–8.
14. Nordly P, Madsen HB, Nielsen HM, Foged C. Status and future prospects of lipid-based particulate delivery systems as vaccine adjuvants and their combination with immunostimulators. Expert Opin Drug Deliv. 2009;6(7):657–72.
15. Hem SL, Hogenesch H, Middaugh CR, Volkin DB. Preformulation studies-The next advance in aluminum adjuvant-containing vaccines. Vaccine. 2010;28(31):4868–70.
16. Jorgensen L, Vermehren C, Bjerregaard S, Froekjaer S. Secondary structure alterations in insulin and growth hormone water-in-oil emulsions. Int J Pharm. 2003;254(1):7–10.
17. Henriksen-Lacey M, Christensen D, Bramwell VW, Lindenstrom T, Agger EM, Andersen P, *et al.* Liposomal cationic charge and antigen adsorption are important properties for the efficient deposition of antigen at the injection site and ability of the vaccine to induce a CMI response. J Control Release. 2010;145 (2):102–8.
18. Kamath AT, Mastelic B, Christensen D, Rochat AF, Agger EM, Pinschewer DD, *et al.* Synchronization of Dendritic Cell Activation and Antigen Exposure Is Required for the Induction of Th1/Th17 Responses. J Immunol. 2012;188(10):4828–37.
19. Davidsen J, Rosenkrands I, Christensen D, Vangala A, Kirby D, Perrie Y, *et al.* Characterization of cationic liposomes based on dimethyldioctadecylammonium and synthetic cord factor from M. tuberculosis (trehalose 6,6′-dibehenate)-a novel adjuvant inducing both strong CMI and antibody responses. Biochim Biophys Acta. 2005;1718(1–2):22–31.
20. Kendrick BS, Dong AC, Allison SD, Manning MC, Carpenter JF. Quantitation of the area of overlap between second-derivative amide I infrared spectra to determine the structural similarity of a protein in different states. J Pharm Sci. 1996;85(2):155–8.
21. Henriksen-Lacey M, Bramwell VW, Christensen D, Agger EM, Andersen P, Perrie Y. Liposomes based on dimethyldioctadecylammonium promote a depot effect and enhance immunogenicity of soluble antigen. J Control Release. 2009;142(2):180–6.
22. Christensen D, Kirby D, Foged C, Agger EM, Andersen P, Perrie Y, *et al.* alpha, alpha′-trehalose 6,6′-dibehenate in non-phospholipid-based liposomes enables direct interaction with trehalose, offering stability during freeze-drying. Biochim Biophys Acta. 2008;1778(5):1365–73.
23. Jeyachandran YL, Mielezarski E, Rai B, Mielczarski JA. Quantitative and qualitative evaluation of adsorption/desorption of bovine serum albumin on hydrophilic and hydrophobic surfaces. Langmuir. 2009;25(19):11614–20.
24. Cedervall T, Lynch I, Lindman S, Berggard T, Thulin E, Nilsson H, *et al.* Understanding the nanoparticle-protein corona using methods to quantify exchange rates and affinities of proteins for nanoparticles. Proc Natl Acad Sci U S A. 2006;104(7):2050–5.
25. Lynch I, Cedervall T, Lundqvist M, Cabaleiro-Lago C, Linse S, Dawson KA. The nanoparticle-protein complex as a biological entity; a complex fluids and surface science challenge for the 21st century. Adv Colloid Interface Sci. 2007;134–135:167–74.
26. Muga A, Mantsch HH, Surewicz WK. Apocytochrome-C interaction with phospholipid-membranes studied by fourier-transform infrared-spectroscopy. Biochemistry. 1991;30(10):2629–35.
27. Persson D, Thoren PEG, Norden B. Penetratin-induced aggregation and subsequent dissociation of negatively charge phospholipid vesicles. FEBS Lett. 2001;505(2):307–12.
28. Papahadjopoulos D, Moscarello M, Eylar EH, Isac T. Effects of proteins on thermotropic phase transitions of phospholipid membranes. Biochim Biophys Acta. 1975;401(3):317–35.
29. Haskard CA, Li-Chan ECY. Hydrophobicity of bovine serum albumin and ovalbumin determined using uncharged (PRODAN) and anionic (ANS(−)) fluorescent probes. J Agric Food Chem. 1998;46(7):2671–7.
30. Bruylants G, Wouters J, Michaux C. Differential scanning calorimetry in life science: thermodynamics, stability, molecular recognition and application in drug design. Curr Med Chem. 2005;12 (17):2011–20.

31. Robertson AD, Murphy KP. Protein structure and the energetics of protein stability. Chem Rev. 1997;97(5):1251–67.
32. Charbonneau DM, Tajmir-Riahi HA. Study on the interaction of cationic lipids with bovine serum albumin. J Phys Chem B. 2010;114(2):1148–55.
33. Norde W, Favier JP. Structure of adsorbed and desorbed proteins. Colloid Surface. 1992;64(1):87–93.
34. Wallace BA. Protein characterisation by synchrotron radiation circular dichroism spectroscopy. Q Rev Biophys. 2009;42(4):317–70.
35. Wallace BA, Teeters CL. Differential absorption flattening optical effects are significant in the circular dichroism spectra of large membrane fragments. Biochemistry. 1986;26(1):65–70.
36. Wallace BA, Mao D. Circular dichroism analyses of membrane proteins: an examination of differential light scattering and absorption flattening effects in large membrane vesicles and membrane sheets. Anal Biochem. 1984;142(2):317–28.
37. Ladokhin AS. FAU - Fernandez-Vidal M, Fernandez-Vidal MF, White SH. CD spectroscopy of peptides and proteins bound to large unilamellar vesicles. J Membr Biol. 2010;236:247–53.
38. Jackson M, Mantsch HH. The use and misuse of ftir spectroscopy in the determination of protein-structure. Crit Rev Biochem Mol Biol. 1995;30(2):95–120.
39. Cawthern KM, Permyakov E, Berliner LJ. Membrane-bound states of alpha-lactalbumin: implications for protein stability and conformation. Protein Sci. 1996;5(7):1394–405.
40. Grudzielanek S, Smirnovas V, Winter R. The effects of various membrane physical-chemical properties on the aggregation kinetics of insulin. Chem Phys Lipids. 2007;149(1–2):28–39.
41. Ingvarsson PT, Yang MS, Nielsen HM, Rantanen J, Foged C. Stabilization of liposomes during drying. Expert Opin Drug Deliv. 2011;8(3):375–88.
42. Peters T. Serum-Albumin. Adv Protein Chem. 1985;37:161–245.
43. Blake CCF, Koenig DF, Mair GA, North ACT, Phillips DC, Sarma VR. Structure of hen egg-white lysozyme - a 3-dimensional fourier synthesis at 2A resolution. Nature. 1965;206(4986):757–61.
44. Stein PE, Leslie AGW, Finch JT, Carrell RW. Crystal-structure of uncleaved ovalbumin at 1.95 A resolution. J Mol Biol. 1991;221(3):941–59.
45. Stevens L. Egg-white proteins. Comp Biochem Physiol B Biochem Mol Biol. 1991;100(1):1–9.